In vitro antibacterial and cytotoxic activity of zinc oxide, iron oxide and silver nanoparticles synthesised from *Artemisia afra*

Bongisiwe Shelembe[1], Roshila Moodley[1,*] and Hafizah Chenia[2]

[1] *School of Chemistry and Physics, University of KwaZulu-Natal, , Durban, South Africa*
[2] *School of Life Sciences, University of KwaZulu-Natal, Durban, South Africa*

ABSTRACT

The synthesis of nanoparticles using medicinal plants is a potential pathway for developing environmentally friendly drugs with minimal side effects. The aim of this study was to isolate heptadecyl-trans-*p*-coumarate from the medicinal plant, *Artemisia afra*, utilise it and its extract to synthesise silver nanoparticles (AgNPs), zinc oxide nanoparticles (ZnONPs) and iron oxide nanoparticles (Fe_2O_3NPs) that were evaluated for antibacterial and cytotoxic activity. AgNPs synthesised from the coumarate and extract were mostly spherical with an average size of 12 nm and 29 nm, respectively. ZnONPs were mostly rods, plates and spheres with average sizes of 31 nm (extract) and 22 nm (coumarate). Fe_2O_3NPs were hexagons and spheres with average sizes of 31 nm (extract) and 24 nm (coumarate). Nanoparticles improved the antibacterial activity of the extract and coumarate against *Escherichia coli, Pseudomonas aeruginosa, Chromobacterium violaceum* and *Staphylococcus aureus*. Shape of nanoparticles influenced activity; rod-shaped ZnONPs and platelet-like Fe_2O_3NPs synthesised using the extract exhibited better antibacterial activity. Spherical ZnONPs synthesised using the coumarate and spherical AgNPs showed greater cytotoxicity. The results suggest a synergistic effect between the metal nanoparticles and capping agents. Overall, this study confirms the use of *Artemisia afra* for the biosynthesis of silver, zinc oxide and iron oxide nanoparticles.

KEYWORDS

***Artemisia annua,* biosynthesis, coumarate, green synthesis, nanomaterials**

Received 11 August 2020, revised 10 March 2021, accepted 24 November 2021

INTRODUCTION

Nanotechnology is the synthesis, design and application of materials and devices with engineered shapes and sizes at the nanoscale level that are used in applications such as medicine, catalysis and environmental chemistry.[1] According to Sahoo et al.[2], nanoparticle-bound drugs have an extended half-life *in vivo*, longer circulation times and convey a high concentration of potent drugs to the target sites. This is due to the reduced particle sizes and high surface to volume ratios.[3] Nanoparticle-bound drugs are easily suspended in liquids and are able to penetrate deep into organs and tissues. Therefore, there is ongoing research on the development of new nanoparticle-bound drugs that are more effective, have reduced side effects and reach their targets.

Artemisia annua (sweet wormwood or qinghao), is a shrub from the Asteraceae family, that has been used in Chinese traditional medicine to kill the malaria parasite, *Plasmodium falciparum* due to the presence of the highly oxygenated sesquiterpene, artemisinin, in its extract.[4] This plant is currently receiving much attention due to its potential activity against severe acute respiratory syndrome coronavirus 2 (SARS-CoV-2). *Artemisia afra*, an underexploited medicinal plant from the same family and genus, is used in South African traditional medicine to treat several medical conditions including chest infections, wounds, cough, fever, malaria, asthma and diabete.[5-6] Preliminary studies on the crude extract of *A. afra* have shown it to possess antibacterial activity against *Mycobacterium aurum* and *Mycobacterium tuberculosis*, anti-histaminic and narcotic analgesic activities.[7]

The exploitation of medicinal plants for the synthesis of metal and metal oxide nanoparticles for drug delivery is considered as green synthesis.[8] Plant secondary metabolites have the potential to reduce metal ions in solution, resulting in the subsequent formation of nanoparticles. Zinc oxide nanoparticles have previously been synthesised from a variety of plant species including *Pongamia pinnata*, and were shown to have good antibacterial and antioxidant activities.[9–10] The combination of metal oxide nanoparticles and phytocompounds are documented to enhance the therapeutic activity of the nanostructure against a wide range of microbial infections.[11] Iron is an important transitional metal due to its magnetic properties that can be exploited in a variety of applications such as sensors, catalysis, environmental and biomedical remediation.[12] For biomedicine, iron oxide nanoparticles are frequently coated with hydrophilic and biocompatible coatings such as polymers that increase the thickness and the radii up to 100 nm, which causes damping of the magnetic resonance signal.[13] The use of phytocompounds, which are biocompatible and yield nanoscale magnetic iron oxide nanoparticles with functionalized surfaces, is a viable alternative.

In this study, we aim to isolate and identify the major secondary metabolite from the extracts of *A. afra,* which would then be used to reduce silver, zinc oxide and iron oxide salts to their nano sizes. The antibacterial and cytotoxic activities of the extract, isolate and synthesised nanoparticles will be compared and evaluated. To date, there have been no reports on the use of *A. afra* for the synthesis of metal nanoparticles.

MATERIALS and METHODS

Collection of plant samples and preparation of aqueous extract

The leaves from *Artemisia afra* were purchased from the Durban Muthi Market, KwaZulu-Natal. The leaves were dried at room temperature for two weeks and crushed using a food processor. Approximately 50 g of crushed leaves was weighed and transferred into a 1000 mL beaker containing 500 mL distilled water, and refluxed at 90 °C for 20 minutes. The extract was cooled and filtered twice through Whatman No. 1 filter paper and stored in a refrigerator at 4 °C until further use.

Isolation and purification of compound from Artemisia afra

The ground leaves from *A. afra* (1 kg) were extracted with methanol (MeOH) for three days using an orbital shaker as described by

*To whom correspondence should be addressed
Email: moodleyrosh@ukzn.ac.za

ISSN 1996-840X Online / South African Chemical Institute / https://saci.co.za/journal

https://doi.org/10.17159/0379-4350/2023/v77a14

Shelembe, Mahlangeni and Moodley.[14] From the MeOH extract, 20 fractions of 10 mL each were collected for each eluent step. Fraction 8 was recrystallized with MeOH to yield the major compound (23 mg).

Synthesis of nanoparticles using the aqueous extract and isolated compound

Nanoparticles were synthesised according to the method described by Singh, Singh and Rawat [15] for zinc oxide nanoparticles (ZnONPs), El-Kassas, Aly-Eldeen and Gharib [8] for iron oxide nanoparticles (Fe_2O_3NPs) and Jyoti, Baunthiyal and Singh [16] for silver nanoparticles (AgNPs). The colour changes of the solution or appearance of a precipitate indicated the formation of nanoparticles. Nanoparticles were only synthesised using the isolated compound and aqueous extract as these particles may be used in biomedical applications.

Silver nanoparticles (AgNPs)

Nanoparticles were synthesised according to the method described by Jyoti, Baunthiyal and Singh.[16] An aqueous solution of silver nitrate (50 mL, 1 mM) was added dropwise (2 mL per minute) to the aqueous plant extract (50 mL). The solution was stirred overnight at room temperature using a magnetic stirrer. A color change from orange to grey-black was observed. The suspended AgNPs were centrifuged at 5000 rpm for 30 minutes, washed several times with deionized water, and dried in an oven for eight hours at 50 °C. For synthesis of AgNPs using the compound, 10 mg of the compound was dissolved in 10 mL of MeOH and reacted with 10 mL of $AgNO_3$.

Zinc oxide nanoparticles (ZnONPs)

A solution of zinc chloride (50 mL, 0.4 M) was added to the aqueous plant extract (50 mL) drop-wise. The solution was stirred at room temperature for 2 h. The pH of the solution was adjusted to 11 by adding a solution of NaOH (1.0 M) drop-wise with constant stirring for 2 h at room temperature. The resulting precipitate was obtained after centrifugation at 5000 rpm for 30 minutes, washing several times with deionized water, and drying in an oven at 100 °C for 2 h.

Antibacterial activity

The antibacterial activity of the nanoparticles synthesised from the aqueous extract of *Artemisia afra* and isolated compounds were tested against a series of bacterial strains including the Gram-negative *Escherichia coli* ATCC 35218 and ATCC 25922, *Pseudomonas aeruginosa* ATCC 27853, *Klebsiella pneumonia* ATCC 700603 and *Chromobacterium violaceum* ATCC 12472, and Gram-positive *Staphylococcus aureus* ATCC 43300 and ATCC 29213 and *Enterococcus faecalis* ATCC 51299 and ATCC 29212, using the well diffusion method.[17] Molten and cooled nutrient Mueller Hinton (MH) (20 mL) agar media was poured into a sterilized petri dish and left overnight at room temperature. Agar plates were bored using a sterile gel borer to make wells of 3 mm diameter. Nanoparticles suspended in distilled water, extract or phytocompound dissolved in 10 % DMSO was loaded into wells (40 µL or 20 µL, 10 mg mL^{-1}) in triplicate. Ampicillin (10 µg per disc) was used as a positive control while sterile water and DMSO was used as negative controls. The disc was placed on Muller Hilton agar plates inoculated with each microorganism. The plates were incubated at 37 °C for 24 hours. After the incubation period, the zone of inhibition was measured (mm).

Cell viability and cytotoxicity testing

The cancerous MCF7 (breast adenocarcinoma) and A549 (human lung adenocarcinoma), and non-cancerous HEK239 (human embryonic kidney) cell lines were obtained from the American Tissue Culture Collection (ATCC) (Virginia, USA). Cells were grown in 25 mL tissue culture flasks in Dulbecco's modified Eagle's minimum essential medium (DMEM) supplemented with foetal bovine serum (FBS) (10 %) with an antibiotic mixture of penicillin (100 µg mL^{-1}) and streptomycin (100 µg mL^{-1}). At approximately 85 % confluence, the cells were harvested using 0.25 % trypsin and seeding in a 25 mL flask. Cells at a seeding cell density of 1.8×10^5 cells per well were plated into a 96-well plate containing 200 µL of medium. The cells were incubated at 37 °C in 5 % CO_2 and 95 % air with 80 % humidity, overnight (eight hours). Thereafter, the medium was removed and freshly prepared medium (100 µL) was added.

Test samples (1 mg) were dissolved or suspended in 20 % DMSO and was further diluted with media to make a total volume of 4 mL. Different concentrations (30, 75, 125 and 250 µg mL^{-1}) were added in triplicate to the cells and incubated for 48 hours at 37 °C. The medium was again removed and a volume of 20 µL of 3-(4,5-dimethylthiazolyl-2)-2,5-diphenyltetrazolium bromide (MTT) solution was added. The solution was incubated at 37 °C for 3 hours. Thereafter, DMSO (100 µL) was added to dissolve the crystal and incubated for 10 minutes. The absorbance was measured at the wavelength of 570 nm and the percent viability was calculated. Standard anticancer drugs, 5-fluorouracil (5FU) and doxorubicin, were used as positive controls and untreated cells as a negative control. The cell viability was calculated using the following equation:

$$\text{Cell viability (\%)} = (A_{\text{sample}}/A_{\text{untreated cells}}) \times 100 \quad (1)$$

RESULTS and DISCUSSION

Structural elucidation of isolated compound from *A. afra*

The compound was isolated as a dark brown solid (23 mg). The ^{1}H NMR spectrum showed two resonances that integrated to two protons each, at δ_H 7.4 (H-5/9) and 6.8 (6/8), indicative of a *p*-substituted benzene ring. Furthermore, two doublets that integrated to one proton each, with resonances at δ_H 7.6 (H-3) and 6.3 (H-2), were indicative of an olefenic group. The resonances between δ_H 1.25-1.06 indicated methyl and methylene groups. The resonance at δ_H 1.25 integrated to 26 protons, indicating 13 methylene groups. The ^{13}C NMR spectrum showed a characteristic resonance of a carbonyl at δ_C 167, which correlated with the proton at δ_H 4.1 (H-1') in the HMBC experiment. The GC-MS spectrum gave a molecular ion peak at *m/z* 401, which corresponds to the molecular formula $C_{26}H_{42}O_3$. The compound had a similar backbone to the coumarate previously isolated from *Ipomoea sepiari*.[18] The ^{1}H NMR spectrum indicated that there is a chain with 16 methylenes. With the data obtained, it can be concluded that the compound is heptadecyl-trans-*p*-coumarate (Figure 1).

Characterisation of nanoparticles

Three metal and metal oxide nanoparticles (ZnONPs, Fe_2O_3NPs and AgNPs) were successfully synthesised using the aqueous extract and isolated compound (heptadecyl-trans-*p*-coumarate) from *A. afra*. A colour change caused by excitation of the surface plasmon resonance (SPR) was indicative of the formation of nanoparticles.[19]

Figure 2 shows the UV-Vis absorption spectra of ZnONPs, Fe_2O_3NPs and AgNPs synthesised from the aqueous extract and isolated compound, respectively. The UV-Vis spectra showed strong absorption peaks at 338 nm (Fe_2O_3NPs) and 279 nm (ZnONPs), which are in agreement with previous studies.[20-21] The UV-Vis spectrum of AgNPs synthesised from the coumarate (413 nm) exhibits a blue shift

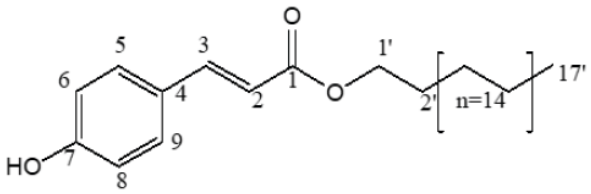

Figure 1. Chemical structures of heptadecyl-trans-*p*-coumarate

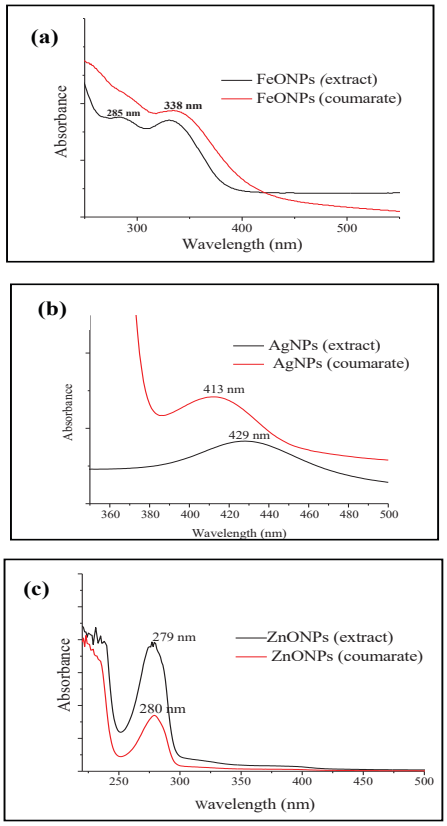

Figure 2. UV-Vis spectra of nanoparticles a) Fe_2O_3NPs, b) AgNPs, c) ZnONPs. synthesised from both the aqueous extract and isolated compound (coumarate)

compared to those synthesised from the aqueous extract (429 nm), which is in agreement with that in literature, indicative of particle shape and size differences with both peaks being relatively broad, indicative of large particle size distribution.[9,22]

The morphology and size of the nanomaterial prepared using the aqueous extract and isolated coumarate were analysed using transmission electron microscopy (TEM) and are presented in Figure 3. The average size represented by the histogram, also represented particle size distribution.

The images demonstrated agglomeration of ZnONPs (Figure 3 (1a, 1b)) prepared using the aqueous extract with a variety of shapes, dominated by spheres, which coagulated to form rods, hexagons and rectangular nanoparticles. Particle sizes (from 150 particles) ranged from 5 to 80 nm, with an average size of 31 nm. Nanoparticles synthesised from the coumarate (Figure 3 (1c, 1d)) showed agglomerated hexagons, triangles, rods and spheres with smaller (6 nm) and larger (48 nm) particles.

Silver nanoparticles synthesised using the aqueous extract showed spherical and irregular shapes with a wide, fairly dispersed, particle size range (Figure 3 (2a, 2b)). The particle size distribution ranged from 4 nm to 24 nm, with an average size of 13 nm. Silver nanoparticles synthesised using the coumarate showed spherical nanoparticles with particle sizes ranging from 25 to 75 nm, with an average size of 29 nm, indicating larger and more monodispersed particles than those synthesised using the aqueous extract thereby supporting the blue shift observed from the UV-Vis data.

The TEM images (Figure 3 (3a, 3b)) of Fe_2O_3NPs synthesised using the aqueous extract, showed the presence of lattice fringes (insert Figure 3 (3a)), which represents the crystalline nature and the distance between the planes. A mixture of irregular platelet-like structures and hexagons with a size range of 5-80 nm and average size of 31 nm was detected. Nanoparticles synthesised using the coumarate, showed agglomerated spheres and rods (Figure 3 (3c, 3d)) and end-capping by phytocompounds (insert Figure 3 (3c)). A 28 nm nanoparticle was capped with phytocompounds that were 2 nm in size. The average particle size was 24 nm and their sizes ranged from 5–85 nm.

The scanning electron microscopy (SEM) coupled with energy dispersive x-ray (EDX) spectroscopy (Figure 4) was further used to confirm the morphology of the synthesised nanoparticles. The selected area electron diffraction (SAED) pattern for ZnONPs synthesised from the aqueous extract (Figure 4 (1a)) showed reflections arranged

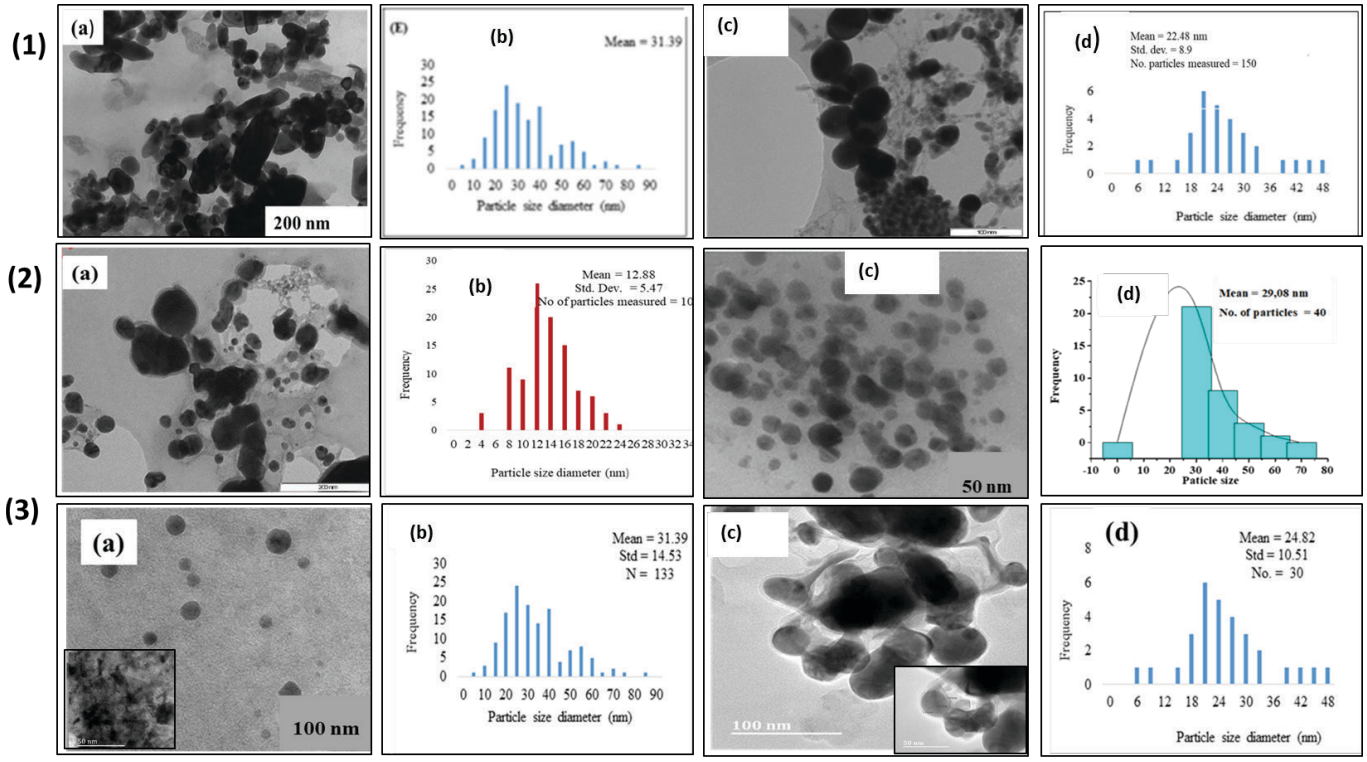

Figure 3. TEM micrographs and particle size distribution histogram from the TEM images of: 1(a&b) ZnONPs synthesised using the aqueous extract; 1(c&d) ZnONPs synthesised using coumarate; 2(a&b) AgNP synthesised using the aqueous extract; 2(c&d) AgNP synthesised using coumarate; 3(a&b) Fe_2O_3NPs synthesised using the aqueous extract; and 3(c&d) Fe_2O_3NPs from coumarate

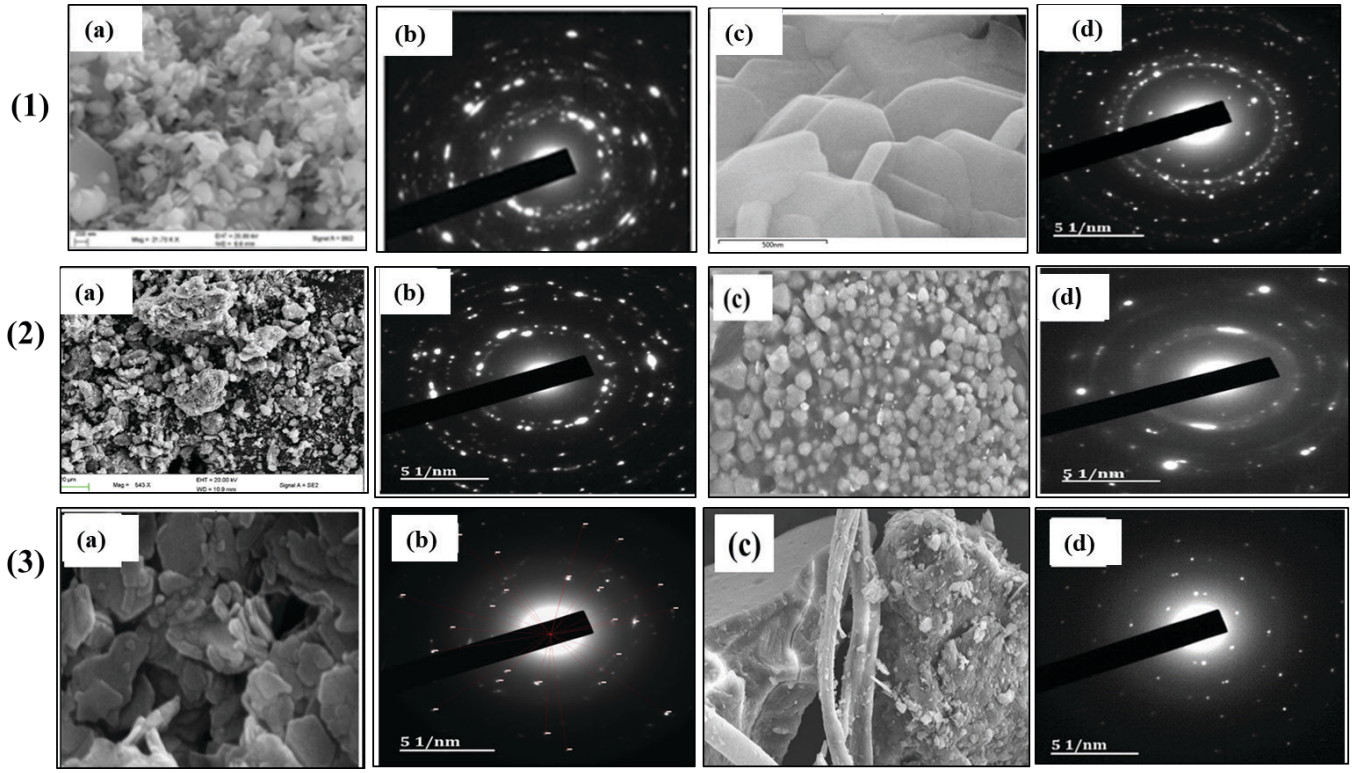

Figure 4. SEM micrograms and their SAED patterns of: 1(a&b) ZnONP from aqueous extract; 1(c&d) ZnONP from coumarate; 2(a&b) AgNP from crude extract; 2(c&d) AgNP from coumarate; 3(a&b) Fe2O3NPs from crude extract; and 3(c&d) Fe2O3NPs from coumarate

in a ring, which is indexed according to the (002), (101), (101), (102) and (103) planes, corresponding to zincite of ZnO (Table 1). The SAED pattern of AgNPs synthesised using the aqueous extract and coumarate (Figure 4 (2a–c)) showed bright spots arranged in circular rings, which can be indexed to reflections from the (111), (200), (220), (311) and (222) planes from the calculated lattice spacing (d) presented (Table 2). The planes correspond to the face centred cubic (fcc) structure of silver.[16, 23]

The SEM micrographs (Figure 4 (3a)) confirmed the hexagon platelet-like particles of Fe_2O_3NPs synthesised using the aqueous extract. The SAED pattern (Figure 4 (3b)) showed bright spots making up a ring. This supports the TEM image and showed the presence of lattice fringes that represent the crystalline nature and the distance between the planes. The calculated reciprocal of the radius from the SAED pattern was used to identify the crystalline phase of the Fe_2O_3NPs. The obtained d-values for the nanoparticles synthesised using the extract (in nm) were 0.33634, 0.2631, 0.25196, 0.2212 and 0.1644 corresponding to (104), (110), (113), (116) and (018) lattice planes, while those synthesised using the coumarate (in nm) were 0.2524, 0.2587, 0.2151, 0.1682 and 0.1615 corresponding to (110), (104), (113), (116) and (018) lattice planes of a α-Fe_2O_3.[2]

The EDX spectrum (Figure 5) of the synthesised nanomaterials confirmed the presence of zinc in ZnONPs (Figure 5a and 5b), iron and oxygen in Fe_2O_3NPs (Figure 5c and 5f) and silver in AgNPs (Figure 5d and 5e). Carbon and oxygen are due to scattering caused by phytocompounds capping the particles, the source of nitrogen was the starting material and gold came from the sample coating used to prevent charge of the specimen. The EDX data of the synthesised Fe_2O_3NPs showed the effect of fluorescence caused by excitation from the Cu k-α energy = 8.046 keV since it has higher energy than Fe, which is 7.112 keV.

Table 1. Structural parameters of synthesised ZnONPs

Miller indices (hkl)	2θ (degrees)	Literature	Coumarate	Aqueous extract
		d-spacing (nm)		
(100)	31.84	0.281	0.280	0.280
(002)	34.52	0.260	0.259	0.259
(101)	36.33	0.247	0.246	0.246
(102)	47.63	0.200	0.190	0.190
(110)	56.71	0.162	0.162	0.162

Table 2. Structural parameters of synthesised AgNPs

Miller indices (hkl)	2θ (degrees)	Literature	Coumarate	Aqueous extract
		d-spacing (nm)		
(111)	38.12	0.235	0.23914	0.2369
(200)	44.27	0.204	0.21126	0.2008
(220)	64.42	0.144	0.1445	0.1442
(311)	77.47	0.123	0.12057	0.12084
(222)	81.53	0.117	0.1198	0.1118

Antibacterial activity

Antibacterial activity of ZnONPs, Fe_2O_3NPs, and AgNPs was tested against both Gram-negative (*E. coli* and *C. violaceum*) and Gram-positive (*S. aureus* and *P. aeruginosa*) bacterial strains. The activity of the test samples was determined by measuring the zones of inhibition using a standard agar-well diffusion method and results are presented in Table 3. The displayed results are only for the test samples that showed inhibitory potential. The aqueous extract and coumarate alone showed no antibacterial activity against all bacterial strains tested except for *C. violaceum*, indicating anti-quorum sensing potential. Reducing metals with both the coumarate and aqueous extract showed better activity. The antibacterial activity of the nanoparticles (capping agent, average size) was found to be in decreasing order of Fe_2O_3NPs (extract, 31 nm) > ZnONPs (extract, 31 nm) > AgNPs (coumarate, 29 nm) > ZnONPs (coumarate, 25 nm) ~ AgNPs (extract, 13 nm) > Fe_2O_3NPs (coumarate, 22.4 nm).

ZnONPs and Fe_2O_3NPs capped with the aqueous extract exhibited

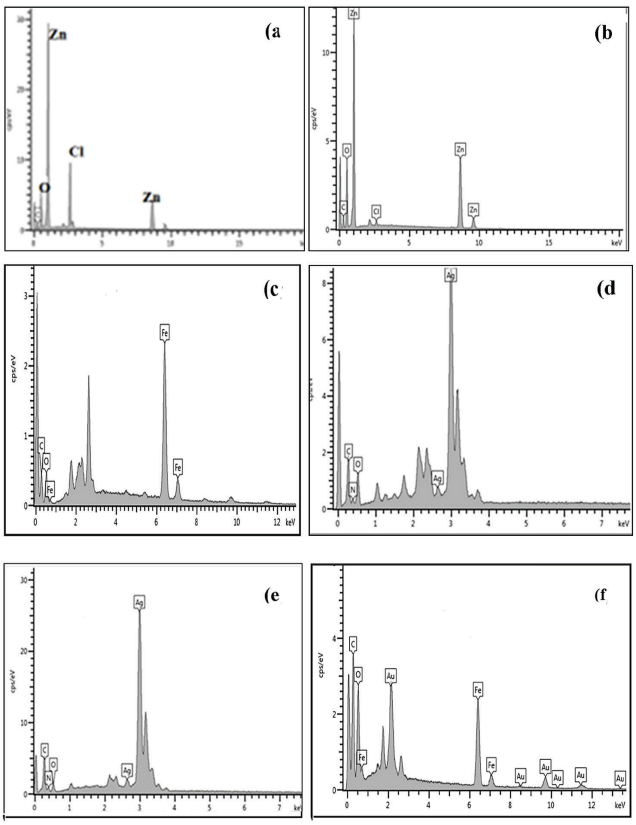

Figure 5. EDX spectrum of nanomaterial a) ZnONPs from aqueous extract, b) ZnONPs from coumarate, c) Fe2O3NPs from aqueous extract, d) AgNPs from aqueous extract, e) AgNPs from coumarate and f) Fe_2O_3NPs from coumarate

better antibacterial activity against both the Gram-negative and Gram-positive strains tested, compared to the aqueous extract alone, with Fe_2O_3NPs having the best activity overall. The antibacterial activity of ZnONPs synthesised using the coumarate showed better activity compared to the coumarate alone for all bacterial strains tested whilst Fe_2O_3NPs had no effect on the coumarate. Previous studies on the effects of various shapes of ZnONPs on toxicity of bacteria showed rods and wires to influence the mechanism of internalization and penetrated the cell walls easier than spherical nanoparticles.[24] This was confirmed by the improved antibacterial activity of ZnONPs capped with the extract that were rods and platelets compared to ZnONPs capped with the coumarate that were spheres and platelets. Iron is one of the essential elements involved in metabolic processes such as respiration, photosynthesis and gene regulation in aerobic organisms. At high concentrations, bacteria tend to absorb iron and reduce it, which in turn, reacts with H_2O_2 forming a hydroxyl radical. The radical damages proteins and nucleic acids of the cell membrane of the bacteria.[25] Fe_2O_3NPs synthesised using the extract produced irregular platelet-like structures and hexagons whilst those synthesised using the coumarate produced a cluster of agglomerated particles with rods; shape affected the activity more than size as the smaller particles capped with the coumarate were less active than the larger ones capped with the extract.

Silver nanoparticles have previously been shown to have good antibacterial activity. In this study, AgNPs improved the antibacterial activity of the extract and coumarate for all bacterial strains tested. AgNPs synthesised with the aqueous extract demonstrated antibacterial potential towards the Gram-negative bacteria, *E. coli* and C. *violaceum*, whilst AgNPs synthesised with the coumarate were active against all bacterial strains tested.

Overall, Fe_2O_3NPs (extract, sizes up to 90 nm), ZnONPs (extract, sizes up to 80 nm) and AgNPs (coumarate, sizes up to 75 nm) were more active than ZnONPs (coumarate, sizes up to 22.5 nm), AgNPs (extract, sizes up to 24 nm) and Fe_2O_3NPs (coumarate, sizes up to 48 nm). The results indicate that larger particles have more antibacterial activity than smaller ones.

According to Alswieleh and Alghamdi [11], the size of the nanoparticles allows them to penetrate the cell wall of the bacteria and interact with cellular elements. Some studies showed size-dependent antibacterial activity with smaller particles having greater bacterial growth inhibition due to their large surface area to volume ratio whilst other studies showed morphology-dependent antibacterial activity.[26–29] Our results show shape or morphology to influence antibacterial activity more than size for ZnONPs, Fe_2O_3NPs and AgNPs against the bacterial strains tested. Therefore, our results agree with those that demonstrate that AgNPs undergo a shape-dependent interaction with bacteria such as *E. coli*.[30]

Cell viability and cytotoxicity testing

Three cell lines (human ambryonic kidney (HEK293), human lung adenocarcinoma (A549) and human breast adenocarcinoma (MCF-7)) were used to evaluate the cytotoxicity of the aqueous extract, isolated compound (coumarate) and their nanoparticles (ZnONPs and AgNPs), using the MTT cell viability assay. Fe_2O_3NPs did not exhibit cytotoxic activity against cancerous cells. Untreated cells were used as

Table 3. Antimicrobial susceptibility (zone of inhibition (mm)) (mean ± SD, n=3) of the aqueous extract of A. afra, isolated coumarate and their synthesised silver nanoparticle (AgNPs), iron oxide nanoparticles (Fe_2O_3NPs) and zinc oxide nanoparticles (ZnONPs) against Gram-negative and Gram-positive bacterial strains at different concentrations (50 and 100 µg mL^{-1}). Ampicillin was used as a positive control

Samples	Gram negative						Gram positive					
	E. coli				*C. violacium*		*S. aureus*				*P. aeruginosa*	
	25922		35218		12472		29213		43300		27853	
Concentration	50	100	50	100	50	100	50	100	50	100	50	100
Aqueous extract	0	0	0	0	12 ± 1.74	13 ± 1.02	0	0	0	0	0	0
AgNPs (extract)	12 ± 0.57	15 ± 0.89	10 ± 1.01	12 ± 2.88	9 ± 0.34	13 ± 0.65	0	12 ± 1.23	0	0	0	0
ZnONPs (extract)	13 ± 0.90	18 ± 2.05	14 ± 1.43	16 ± 0.55	19 ± 0.98	19 ± 2.34	20 ± 1.54	24 ± 0.86	23 ± 2.09	24 ± 1.98	12 ± 2.56	14 ± 0.97
Fe_2O_3NPs (extract)	16 ± 0.89	17 ± 0.93	20 ± 1.00	24 ± 1.23	20 ± 0.98	21 ± 0.86	20 ± 2.34	23 ± 1.45	21 ± 0.87	23 ± 0.46	18 ± 0.85	19 ± 1.54
Coumarate	0	10	0	0	0	11 ± 0.87	0	0	0	0	0	0
AgNPs (coumarate)	14 ± 0.82	16 ± 1.08	13 ± 1.11	13 ± 0.86	14 ± 0.97	17 ± 1.12	13 ± 0.95	15 ± 1.02	17 ± 0.99	18 ± 1.08	11 ± 0.87	14 ± 0.95
ZnONPs (coumarate)	10 ± 1.32	10 ± 1.02	0	0	12 ± 0.97	0	12 ± 1.07	16 ± 1.07	10 ± 0.89	12 ± 1.22	0	0
Fe_2O_3NPs (coumarate)	0	0	0	0	0	10 ± 0.98	0	0	0	0	0	10 ± 0.80
Ampicillin	22 ± 2.76		0		0		20 ± 1.05		0		0	

the negative control and 5-FU as the positive control. The results in Figure 6 indicate that all the test samples reduced cell viability for most of the cell lines.

The coumarate displayed selective cytotoxicity towards the cancerous A549 without being cytotoxic against the non-cancerous HEK293 and with moderate cytotoxicity against the cancerous MCF-7 cell lines. When treated with the extract, cell viability of both cancerous and non-cancerous cell lines was greater than 80 %, at low concentrations. Cell growth did not go below 50 % in all cases at high concentrations, thereby indicating moderate cytotoxicity. These results confirm the antagonistic effects of inactive compounds present in the extract that inhibit the cytotoxic activity of active compounds, in this case the coumarate. A possible explanation for the activity of the coumarate could be that the chain enhances its lipophilicity and hence its permeability whilst the cells provide an environment for hydrolysis of the ester into a weak acid that improves activity.[31] Previous studies have also shown coumarins to have good anticancer activity against MCF-7 and Caco-2 cell lines.[31]

AgNPs synthesised using the coumarate displayed non-selectivity with it being highly cytotoxic against the cancerous A549 and non-cancerous HEK293 and moderately cytotoxic against the cancerous MCF-7 cell lines. AgNPs synthesised using the extract also exhibited non-selectivity with good cytotoxicity against all cell lines tested. ZnONPs synthesised using the coumarate were not as active as the AgNPs against the cancerous cell lines. However, at low concentrations they were more selective towards the cancerous A549 (cell viability < 20%) than non-cancerous HEK293 (cell viability > 75 %) cell lines. ZnONPs synthesised using the extract were mostly inactive against the cancerous cell lines.

Contrary to antibacterial activity, ZnONPs synthesised using the coumarate that were mostly spherical were more cytotoxic than the rod shaped ZnONPs synthesised using the extract. Similarly, AgNPs synthesised using the extract and coumarate that were mostly spherical were highly cytotoxic.

The results showed cytotoxic activity against HEK293 to be in decreasing order of AgNPs (coumarate) > ZnONPs (coumarate) > AgNPs (extract) > ZnONPs (extract) > coumarate > extract; against A549 to be in decreasing order of AgNPs (coumarate) > coumarate > ZnONPs (coumarate) > AgNPs (extract) > 5-FU > extract > ZnONPs (extract) and for MCF-7 to be in decreasing order of AgNPs (coumarate) > 5-FU > coumarate > ZnONPs (coumarate) > extract > AgNPs (extract) > ZnONPs (extract). The results suggest a synergistic effect between the metal nanoparticles and capping agents.

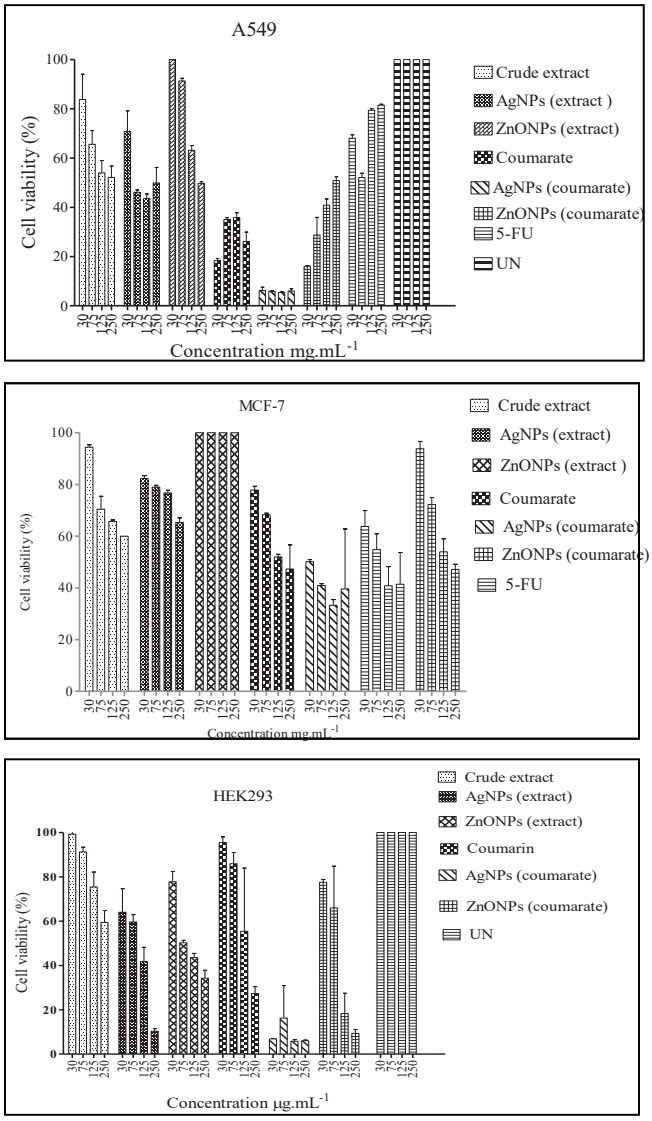

Figure 6: MTT cell viability results (mean ± SD, n=3) for cancerous A549 (human lung carcinoma), MCF-7 (human breast carcinoma) and non-cancerous HEK293 (human embryonic kidney) cell lines after treating with the extract of A. afra, coumarate, their nanoparticles (ZnONPs and AgNPs), 5-fluorouracil (5-FU, positive control) and untreated cells (UN, negative control)

CONCLUSION

In this study, heptadecyl-trans-*p*-coumarate was isolated for the first time from *A. afra*. The biomolecules in *A. afra* reduced and stabilized silver, zinc and iron salts to form their respective AgNPs, ZnONP and Fe_2O_3NPs. ZnONPs and Fe_2O_3NPs synthesised with the extract showed better antibacterial activity than those synthesised with the coumarate; AgNPs synthesised with the coumarate showed better antibacterial activity than those synthesised with the extract. The results indicate that larger particles have more antibacterial activity than smaller ones and that shape was a determinant of activity more than size. AgNPs capped with the coumarate showed better cytotoxic potential against A549 (human lung adenocarcinoma) compared to the biomolecule alone. Synergistic effects were observed for cytotoxicity between the synthesised nanoparticles and the active biomolecules. Overall, this study confirms that the medicinal plant species, *A. afra,* could be used for the biosynthesis of AgNPs, ZnONPs and Fe_2O_3NPs. It also provides a scientific basis for the ethno-medicinal use of the plant to treat various ailments

AUTHOR CONTRIBUTIONS

Bongisiwe Shelembe: Investigation, data curation, methodology, formal analysis, writing - original draft preparation.
Roshila Moodley: Conceptualization, supervision, validation, writing – review and editing, funding acquisition.
Hafizah Chenia: Methodology, data curation, writing – review and editing.

ACKNOWLEDGMENTS

The authors are grateful to the University of KwaZulu-Natal for their resources. This research was funded by the National Research Foundation (NRF) through Prof. Roshila Moodley (Grant number 114008, ORCID iD 0000–0001–7296–0519) and Dr Bongisiwe Shelembe (Grant numbers 95100 and 111234, ORCID iD 0000-0002-1506-5582). We would also like to acknowledge the UKZN Nanotechnology Platform.

ORCID IDs

Roshila Moodley: https://orcid.org/0000-0001-7296-0519
Hafizah Chenia: https://orcid.org/0000-0001-9753-6394

REFERENCES

1. Rashid NB, Abdulsattar SA, Hussain DH. Preparation and characterisation of tiopronin gold nanoparticles. J. App. Chem. 2016;9:61–67.
2. Sahoo SK, Agarwal K, Singh AK, Polke BG, Raha KC. Characterisation of γ- and α-Fe_2O_3 nano powders synthesised by emulsion precipitation-calcination route and rheological behaviour of α-Fe_2O_3. Int J Eng Sci Technol. 2010;2:118–126.
3. Press D. High-energy ball milling technique for ZnO nanoparticles as antibacterial material. Int J Nanomedicine. 2011;6:863–869.
4. Enserink M. Source of new hope against malaria is in short supply. Science. 2005;307(5706):33. https://doi.org/10.1126/science.307.5706.33
5. Gakuba E. Isolation and characterisation of secondary metabolites of two Asteraceae species, *Artemisia afra* and *Elytropappus rhinocerotis*, [MSc thesis]. University of KwaZulu-Natal, Durban, South Africa. 2019.
6. Mukinda JT, Syce JA. Acute and chronic toxicity of the aqueous extract of *Artemisia afra* in rodents. J Ethnopharmacol. 2007;112(1):138–144. https://doi.org/10.1016/j.jep.2007.02.011
7. Patil GV, Dass SK, Chandra R. *Artemisia afra* and modern diseases. J Pharmacogenomics Pharmacoproteomics. 2011;2:1–22. https://doi.org/10.4172/2153-0645.1000105
8. El-Kassas HY, Aly-Eldeen MA, Gharib SM. Green synthesis of iron oxide (Fe_3O_4) nanoparticles using two selected brown seaweeds: characterisation and application for lead bioremediation. Acta Oceanol Sin. 2016;35(8):89–98. https://doi.org/10.1007/s13131-016-0880-3
9. Sundrarajan M, Ambika S, Bharathi K. Plant-extract mediated synthesis of ZnO nanoparticles using *Pongamia pinnata* and their activity against pathogenic bacteria. Adv Powder Technol. 2015;26(5):1294–1299. https://doi.org/10.1016/j.apt.2015.07.001
10. Nagajyothi PC, Sreekanth TVM, Tettey CO, In Y, Heung S. Bioorganic and medicinal chemistry letters of ZnO nanoparticles using *Coptidis Rhizoma*. Bioorg Med Chem Lett. 2014;1:2–7.
11. Alzahrani K, Niazy A, Alswieleh A, Wahab R, El-Toni A, Alghamdi H. Antibacterial activity of trimetal (CuZnFe) oxide nanoparticles. Int J Nanomedicine. 2017;13:77–87. https://doi.org/10.2147/IJN.S154218
12. Teja AS, Koh P. Synthesis, properties, and applications of magnetic iron oxide nanoparticles. Prog Cryst Growth Charact Mater. 2009;55(1-2):22–45. https://doi.org/10.1016/j.pcrysgrow.2008.08.003
13. Salunkhe AB, Khot VM, Ruso JM, Patil SI. Synthesis and magnetostructural studies of amine functionalized superparamagnetic iron oxide. RSC Advances. 2015;5(24):18420–18428. https://doi.org/10.1039/C5RA00049A
14. Shelembe B, Mahlangeni NT, Moodley R. Secondary metabolites isolated from two medicinal plant species, *Bridelia micrantha* and *Sideroxylon inerme* and their antioxidant activities. Adv. Nat. Sci.: Nanotechnol. 2019;10:1–9.
15. Singh K, Singh J, Rawat M. Green synthesis of zinc oxide nanoparticles using *Punica granatum* leaf extract and its application towards photocatalytic degradation of Coomassie brilliant blue R-250 dye. SN Appl Sci. 2019;1:624. https://doi.org/10.1007/s42452-019-0610-5
16. Jyoti K, Baunthiyal M, Singh A. Characterisation of silver nanoparticles synthesised using *Urtica dioica* Linn. leaves and their synergistic effects with antibiotics. J. Radiat. Res. Appl. Sci. 2015;9:217–227.
17. Balouiri M, Sadiki M, Ibnsouda SK. Methods for in vitro evaluating antimicrobial activity: A review. J Pharm Anal. 2016;6(2):71–79. https://doi.org/10.1016/j.jpha.2015.11.005
18. Singh NK, Singh VP. Isolation, characterisation and antioxidant activity of dodecyl-*p*-coumarate from *Ipomoea sepiaria*. J Chem Pharm Res. 2014;6:564–569.
19. Raj A, Lawrence R, Lawrence K, Silas N. Green synthesis and characterization of silver nanoparticles from leaf extracts of *Rosa indica* and its antibacterial activity against human pathogen bacteria. Orient J Chem. 2018;34(1):326–335. https://doi.org/10.13005/ojc/340135
20. Viju Kumar VG, Prem AA. Green synthesis and characterisation of iron oxide nanoparticles using*Phyllanthus niruri* extract. Orient J Chem. 2018;34:2583–2589. https://doi.org/10.13005/ojc/340547
21. Fakhari S, Jamzad M, Habiri Fard H. Green synthesis of zinc oxide nanoparticles: a comparison. Green Chem Lett Rev. 2019;12(1):19–24. https://doi.org/10.1080/17518253.2018.1547925
22. Abdel-Hafez SII, Nafady NA, Abdel-Rahim IR, Shaltout A M, Mohamed A M. Biogenesis and optimisation of silver nanoparticles by the endophytic fungus *Cladosporium sphaerospermum*. Int. J. Nano. Chem. 2016;2:11–19. https://doi.org/10.18576/ijnc/020103
23. Mehta BK, Chhajlani M, Shrivastava BD. Green synthesis of silver nanoparticles and their characterisation by XRD. J Phys Conf Ser. 2017;836: 012050. https://doi.org/10.1088/1742-6596/836/1/012050
24. Yang W, Shen C, Ji Q, An H, Wang J, Liu Q, Zhang Z. Food storage material silver nanoparticles interfere with DNA replication fidelity and bind with DNA. Nanotechnology. 2009;20(8):085102. https://doi.org/10.1088/0957-4484/20/8/085102
25. Sun J, Hutchins DA, Feng Y, Seubert EL, Caron DA, Fu FX. Effects of changing pCO_2 and phosphate availability on domoic acid production and physiology of the marine harmful bloom diatom Pseudo-nitzschia multiseries. Limnol Oceanogr. 2011;56(3):829–840. https://doi.org/10.4319/lo.2011.56.3.0829
26. Reddy Pullagurala VL, Adisa IO, Rawat S, Kim B, Barrios AC, Medina-Velo IA, Hernandez-Viezcas JA, Peralta-Videa JR, Gardea-Torresdey JL. Finding the conditions for the beneficial use of ZnO nanoparticles towards plants-A review. Environ Pollut. 2018;241:1175–1181. https://doi.org/10.1016/j.envpol.2018.06.036
27. Tavakoli S, Kharaziha M, Ahmadi S. Green synthesis and morphology dependent antibacterial activity of copper oxide nanoparticles. J. Nanostruct. 2019;9(1):163–171.
28. Wang X, Wu HF, Kuang Q, Huang RB, Xie ZX, Zheng LS. Shape-dependent antibacterial activities of Ag2 O polyhedral particles. Langmuir. 2010;26(4):2774–2778. https://doi.org/10.1021/la9028172
29. Talebian N, Amininezhad SM, Doudi M. Controllable synthesis of ZnO nanoparticles and their morphology dependent antibacterial and optical properties. J Photochem Photobiol B. 2013;120:66–73. https://doi.org/10.1016/j.jphotobiol.2013.01.004
30. Pal S, Tak YK, Song JM. Does the antibacterial activity of silver nanoparticles depend on the shape of the nanoparticle? a study of the gram-negative bacterium *Escherichia coli*. Appl Environ Microbiol. 2007;73(6):1712–1720. https://doi.org/10.1128/AEM.02218-06
31. Bodede B, Shaik S, Singh M, Moodley R. Phytochemical analysis with antioxidant and cytotoxicity studies of the bioactive principles from *Zanthoxylum capense* (small knobwood). Anticancer Agents Med Chem. 2017;17(4):627–634. https://doi.org/10.2174/1871520616666160627091939